

# Integrated impurity diagnostic package for magnetic fusion experiments

D. Stutman,<sup>a)</sup> M. Finkenthal,<sup>b)</sup> and H. W. Moos  
*Johns Hopkins University, Baltimore, Maryland 21218*

K. B. Fournier  
*Lawrence Livermore National Laboratory, Livermore, California 94550*

R. Kaita, D. Johnson, and L. Roquemore  
*Princeton Plasma Physics Laboratory, Princeton, New Jersey 08543*

(Presented on 10 July 2002)

We develop an integrated instrumental and computational package for the diagnosis of impurity content,  $Z_{\text{eff}}$  profile, particle transport, and magnetohydrodynamics activity in magnetic fusion experiment plasmas. The package includes broadband filtered arrays of absolute (AXUV) photodiodes, a transmission grating imaging spectrometer measuring up to 20 chords across the discharge and having a few angstrom spectral resolution, together with an atomic physics database coupled with an impurity transport code. The atomic physics database is based on *ab initio* computations with the Hebrew University Lawrence Livermore atomic code. The package is designed for the diagnostic of sub-keV plasmas having predominantly low- $Z$  impurities (C, B, and O) together with trace metals. A preliminary version is being tested on the National Spherical Torus Experiment spherical torus at the Princeton Plasma Physics Laboratory, using the ultrasoft x-ray imaging system and a grazing incidence spectrometer. Representative results from non-H-mode discharges are presented. © 2003 American Institute of Physics. [DOI: 10.1063/1.1538327]

## I. INTRODUCTION

Spectroscopic measurements in the  $\approx 1\text{--}2000$  Å range coupled with atomic physics and particle transport computations played an important role in assessing the impurity behavior in the early magnetic fusion energy (MFE) experiments.<sup>1</sup> With the advent of beam heated large tokamaks using low- $Z$  wall materials, Charge exchange recombination spectroscopy (CHERS) has largely replaced “passive” spectroscopy in this task. A simple measurement of the effective impurity charge ( $Z_{\text{eff}}$ ) using the visible or infrared continuum is also possible in these devices.<sup>2</sup>

The recent emergence of smaller scale experiments exploring fusion concepts alternate to the conventional tokamak (e.g., the spherical torus,<sup>3</sup> or the “electric Tokamak”<sup>4</sup>) has, however, renewed the need to characterize impurities in sub-keV temperature plasmas without relying on neutral beams. Even in experiments where CHERS is available, the potential for large poloidal asymmetries in the impurity distribution makes desirable a complementary impurity diagnostics.<sup>5</sup> Finally, the visible continuum  $Z_{\text{eff}}$  measurement is also difficult in these experiments, due to the possible contamination of the spectral window of interest with lines from incompletely stripped impurities.

The spectrum emitted by these colder plasmas extends from the ultrasoft x rays (USXR,  $\approx 10\text{--}300$  Å) to the vacuum ultraviolet and is often more complex than that of large hot tokamaks. A synthetic USXR spectrum computed for a typical beam heated National Spherical Torus Experiment

(NSTX) plasma ( $\langle T_e \rangle \approx 0.6$  keV) is illustrated in Fig. 1, showing that strong low- $Z$  impurity lines and continua can mix with faint but numerous lines emitted by trace  $L$ -shell metallic ions.

The Johns Hopkins Plasma Spectroscopy Group is developing an integrated instrumental and computational package for impurity diagnostic in this type of plasmas. The package is based on simultaneous measurements of the USXR emission with filtered photodiode arrays and a transmission grating imaging spectrometer, coupled with atomic physics and impurity transport calculations. At the same time with the impurity measurements, the fast photodiode response enables imaging of magnetohydrodynamics (MHD) perturbations. Similar techniques have been applied in large tokamaks using the less complex soft x-ray (SXR,  $\approx 1\text{--}10$  Å) emission.<sup>6</sup>

Section II of the article summarizes the instrumentation included in the package. Section III describes its computational basis, while the final section presents example results obtained using the USXR system developed by our group for the National Spherical Torus Experiment.<sup>7</sup>

## II. INSTRUMENTATION PACKAGE

The main tool in the diagnostic package is a set of absolute (AXUV) photodiode arrays filtered with  $K$ - and  $L$ -shell bandpass filters and viewing a poloidal cross section of the plasma, as shown in Fig. 2.<sup>7</sup> The arrays can measure with good spatial and temporal resolution (a few cm and several  $\mu\text{s}$ ), but low-energy resolution (hundreds of eV), the absolute intensity of the line and continuum emission in a few spectral ranges. The use of absolute photodiodes offers

<sup>a)</sup>Electronic mail: stutman@pppl.gov

<sup>b)</sup>Permanent address Racah Institute of Physics, Hebrew University, Jerusalem 91904.

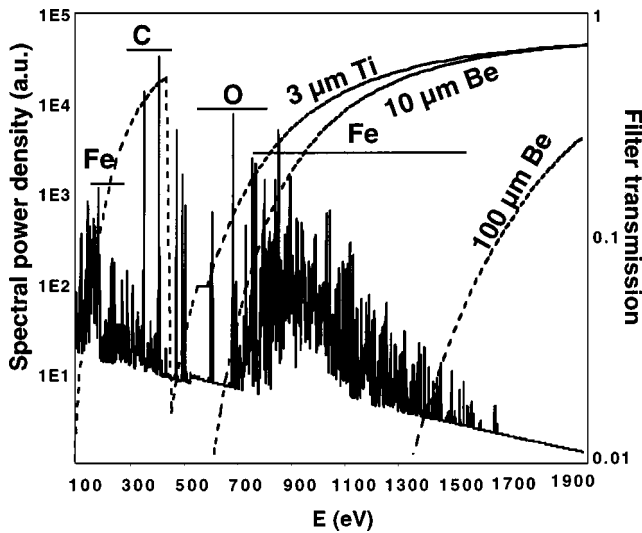


FIG. 1. Synthetic line-of-sight spectrum of NSTX beam heated discharge ( $\langle T_e \rangle \approx 0.6$  keV) computed with the model in Sec. III and assuming 1.5% C, 0.25% O, and 0.02% Fe impurity. Overlaid is the transmission of the filters used for multicolor impurity measurements on NSTX.

the advantage of a uniform spectral response in the USXR range.<sup>7</sup> With an approximate knowledge of the emission spectrum, measurements of the total radiated power in the range  $\approx 0.01$ –10 keV are also possible with the arrays.<sup>8</sup>

For impurity diagnostic the arrays are operated in a “multicolor” configuration in which each array is differently filtered. The rationale behind this technique is illustrated also in Fig. 1, where the transmission of 0.3  $\mu\text{m}$  Ti, 10  $\mu\text{m}$  Be, and 100  $\mu\text{m}$  Be foils is overlaid with the synthetic sub-keV spectrum. As seen, the filters allow roughly discriminating between the peripheral C line emission, the core C con-

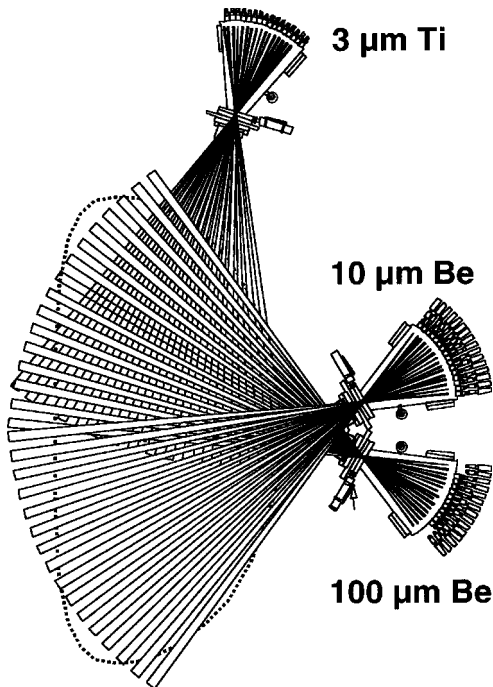


FIG. 2. Layout of the USXR arrays on NSTX in the multicolor configuration used for impurity diagnostic. A fourth array measures at a different toroidal location.

### Asymmetry coefficients

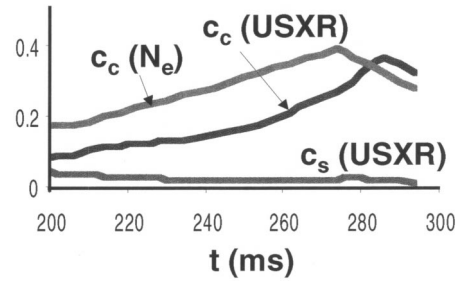


FIG. 3. Evolution of the coefficients describing the poloidal asymmetry in the USXR emissivity (up/down  $c_s$  and in/out  $c_c$ ) during an L-mode discharge in the NSTX. The in/out electron density asymmetry is also shown for comparison.

tinuum, and the core metal emission. This technique can also be used to separate peripheral and core charge states of injected impurities in perturbative transport experiments.<sup>9</sup>

Ideally, one would use tomographic techniques to obtain the two-dimensional (2D) emissivity in each spectral range. The angular coverage in the “multicolor” configuration is, however, limited. To invert the USXR data we assume instead that the emissivity is a flux surface function and fit it using the up/down profiles measured with the horizontal arrays and the magnetic reconstruction. This procedure was validated through an assessment of the poloidal asymmetries, in which we operated the USXR system with identical filters on each array and measured the poloidal variation in the emissivity

$$e(r, \theta) = \left[ \sum c_n r^n \right] [1 + c_s \sin(\theta) + c_c \cos(\theta)]. \quad (1)$$

The measured asymmetry coefficients  $c_s$  and  $c_c$  indicate that the up/down asymmetry is negligible in non-H-mode discharges (Fig. 3), thus enabling the above inversion technique. The inversion of the USXR data in H-mode discharges is less accurate, due to somewhat larger up/down asymmetries and also to the limited spatial resolution of the USXR system.

The second component in the instrumentation package is a novel imaging USXR spectrometer, based on a normal incidence transmission grating coupled to the 2D detector. The principle of the instrument is illustrated in Fig. 4, while details and prototype tests are described in Ref. 10. The spectrometer can simultaneously measure the brightness profile of all spectral lines in the  $\approx 10$ –300  $\text{\AA}$  range, with  $\approx a/20$  spatial resolution ( $a$ , device minor radius), several ms time resolution, and up to  $\approx 3$   $\text{\AA}$  spectral resolution (when using a 10 000 l/mm grating). The space–time resolved electron and beam excited spectra are then used in the package to constrain the modeling of the USXR array data, in particular, the relative impurity fractions. For example, the relative intensity of the  $H_\alpha$  transitions from low-Z impurities (e.g., C VI 182  $\text{\AA}$  vs O VIII 102  $\text{\AA}$ ) provides a simple measure of their fractional concentration in beam heated discharges.

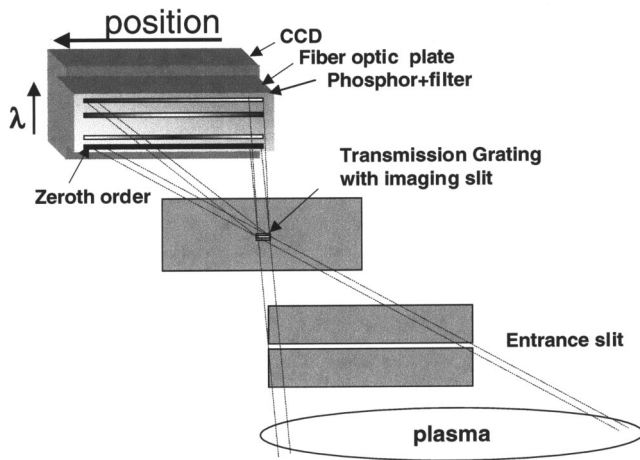


FIG. 4. Conceptual schematic of the imaging transmission grating spectrometer. The narrow fan of rays defined by the entrance and imaging slits is dispersed by a high-resolution transmission grating onto a two-dimensional USXR detector.

### III. COMPUTATIONAL PACKAGE

At the core of the computational package is an atomic database generated using the Hebrew University Lawrence Livermore atomic code (HULLAC) suite of codes.<sup>11</sup> HULLAC can compute in a relativistic approximation the energy levels, radiative transition probabilities, and collisional excitation coefficients for all charge states of a given impurity, up to high principal quantum numbers (typically,  $n \leq 5$ ). Ionization and recombination coefficients between charge states can also be generated. The HULLAC predictions have been benchmarked in a series of experiments on large tokamaks.<sup>12</sup>

In our package, HULLAC is used to compute in the collisional-radiative approximation the power emitted by each transition of a given charge state, for a range of electron temperatures between 50 eV and several keV. Tens of thousands of transitions are involved in modeling the intermediate charge states of iron group metals, for example. The computed power spectra are then convoluted with the filter and diode spectral response and integrated over energy. The result is a set of line emission radiative coefficients for each filter and each charge state of all the impurities of interest. An example is illustrated in Fig. 5 for Cu ions. A similar path is used to compute continuum radiative coefficients, using formulas developed in Ref. 13.

The charge state density for each impurity is computed using the one-dimensional multiple ionization state transport (MIST) impurity transport code<sup>14</sup> and the experimental electron temperature and density profiles, mapped onto the multiple ionization state transport (MIST) space using the magnetic flux surfaces. Ionization, recombination, and charge exchange with beam and thermal neutrals are currently computed using the models and atomic data in MIST. HULLAC computed ionization/recombination data have also been investigated for a few elements.<sup>12</sup>

The emissivity is then obtained by multiplying the radiative coefficient at the local electron temperature with the impurity charge state density and electron density and by mapping back on the flux surfaces. Finally, the cross-field

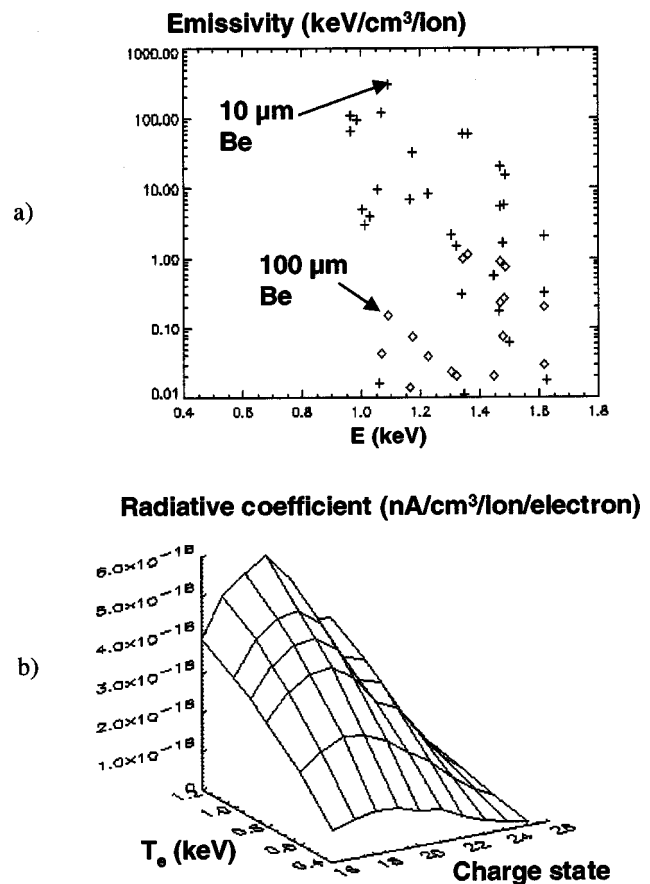


FIG. 5. (a)  $\text{Cu}^{19+}$  spectral emissivity at  $T_e = 0.9$  keV,  $n_e = 10^{13} \text{ cm}^{-3}$  for two Be filters. (b) Line emission radiative coefficient computed using HULLAC for  $\text{Cu}^{16+}$  to  $\text{Cu}^{26+}$  (diode current units are used in our model for simplicity).

transport is varied through the diffusive and convective coefficients  $D$  and  $V$ , in order to reproduce the measured USXR profiles and calibrated high-resolution spectra. The simulations can, therefore, estimate the transport coefficients simultaneously with producing the impurity profiles. In steady-state conditions, however, only the radial dependence of the net particle flux (i.e., a function of  $D/V$ ) can be determined.<sup>15</sup> Time-dependent simulations can nevertheless estimate the magnitude of the transport coefficients, as illustrated below.

## IV. TEST RESULTS FROM NSTX

### A. Intrinsic impurity content and profile measurements

A test version of the above package has been applied for a variety of measurements on the NSTX spherical torus at Princeton.<sup>3</sup> The line-averaged electron temperature in beam heated discharges in this device is in the 0.5–0.9 keV range. Graphite plasma facing components, boronization, and high-temperature bakeout are used in NSTX to limit the oxygen and metal impurity content.

To determine the relative impurity fractions and constrain the modeling of the array data in the test version of the package, we used a photometrically calibrated grazing incidence USXR spectrometer viewing along a central chord

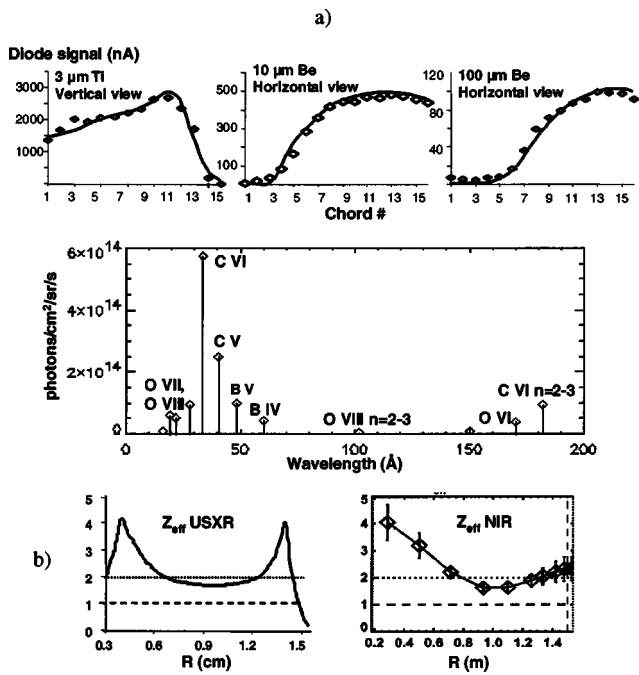


FIG. 6. (a) Measured ( $\diamond$ ) and computed ( $\blacksquare$ ) USXR profiles in three spectral ranges and comparison between measured and simulated high-resolution USXR spectrum. (b) Comparison between  $Z_{\text{eff}}$  profile obtained from simulations of USXR data and that obtained from near-infrared measurements using the Thomson scattering background. The in/out asymmetry is not included in the USXR computation.

across the heating beam.<sup>16</sup> A prototype multichordal transmission grating spectrometer is currently being tested on NSTX (see Ref. 10 for first results).

An example result of modeling the whole USXR data set is presented in Fig. 6, for a discharge having C, B, and O as main impurities. The profiles measured by the USXR arrays in three energy ranges and the line intensities measured by the high-resolution spectrometer are well reproduced. In addition, the  $Z_{\text{eff}}$  estimated from the USXR data compares fairly well with that deduced from near-infrared continuum measurements. The USXR model does not account for the in/out asymmetry.

Carbon profiles estimated through such computations for Ohmic, *L*- and *H*-mode neutral beam heated discharges are illustrated in Fig. 7. The Ohmic profiles evidence impurity accumulation in the core, while the *H*-mode profiles indicate accumulation at the periphery. The *L*-mode profiles exhibit a “step” in the C density at midradius, first suggesting the existence of a discontinuity in impurity transport.<sup>16</sup>

**B. “Two-color” electron temperature estimates**

The consistency between the  $T_e$  profiles measured by laser scattering and the USXR profiles in different energy ranges has also been evaluated using the “multicolor” setup in Fig. 2. The measurements were prompted by a possible discrepancy between the laser results and those obtained using high-resolution x-ray spectroscopy. The USXR estimate obtained by simultaneously fitting the profiles in the  $E > 0.6$  keV and  $E > 1.4$  keV energy ranges agrees within  $\approx 15\%$  with the laser measurements.

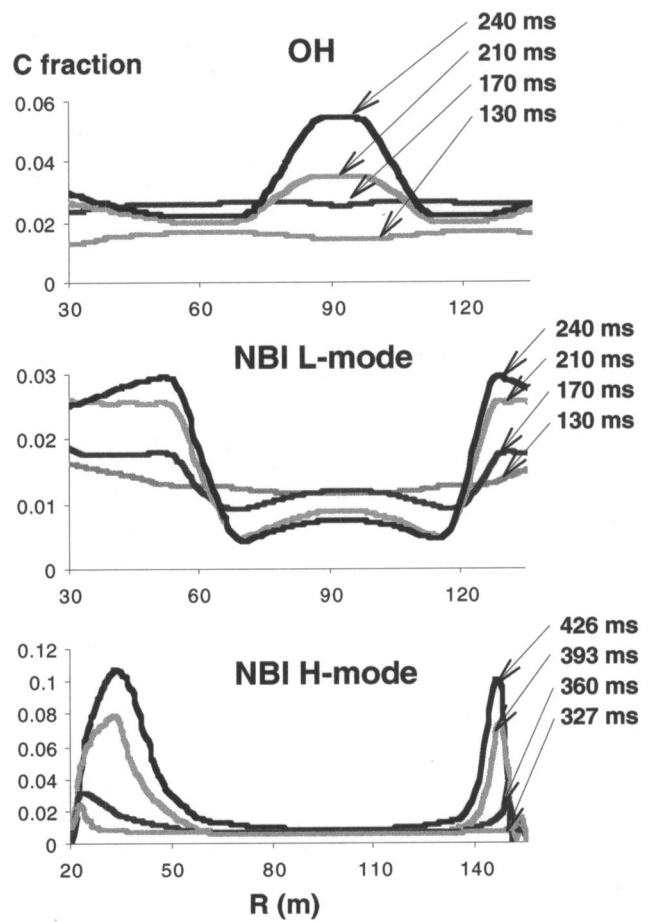


FIG. 7. Estimated evolution of C profiles in 1 MA Ohmic and neutral beam injection heated (*L*- and *H*-modes) NSTX plasma. (Ohmic and *L*-mode data measured before the error field correction on NSTX.)

Our analysis shows there are two main sources of error when applying the two-color technique to the sub-keV plasmas in discussion: spectral contamination by trace metals and the variation in filter thickness with chord angle. Of these, our modeling indicates that the first one can be accurately assessed. Thus, as shown in Fig. 8(a), the presence of trace metal impurities in a several hundred eV plasma significantly increases the ratio between the  $E > 0.6$  keV and  $E > 1.4$  keV signals (the “Be 10/Be 100” ratio), and thus leads to an underestimate of the true temperature. At the same time, however, bright resonance lines emitted by *M*- and *L*-shell metal ions from the plasma core (e.g., Mg-like Fe at 284 Å, or Na-like Fe at 335 Å) should appear in the 100–350 Å spectral region. As illustrated by the calibrated NSTX spectrum in Fig. 8(b), it is then possible to assess the spectral purity of the two-color measurement down to very low metal concentrations, by measuring the intensity of these transitions.

More difficult to avoid is the error due to the change in filter thickness. The computations in Fig. 9 show that for a few hundred eV average temperature plasma this effect induces a  $\leq 8\%$  systematic error in the Be 10/Be 100 ratio. This, in turn, limits the overall accuracy of the  $T_e$  estimate to the above-quoted value. In principle, however, this effect can

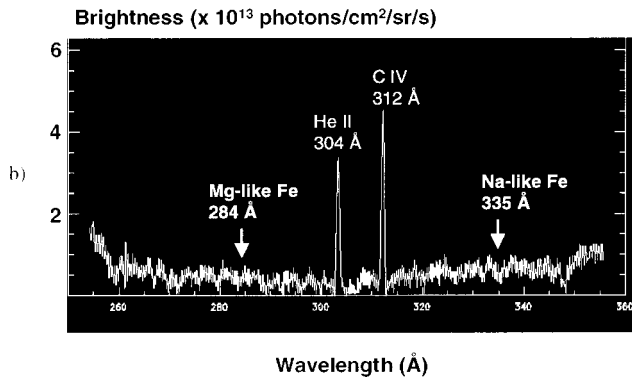
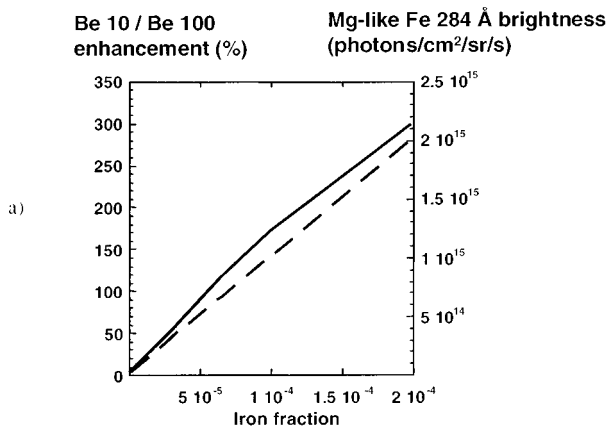


FIG. 8. (a) Enhancement of the Be 10/Be 100 ratio and brightness of Mg-like Fe 284 Å transition as a function of iron concentration in a typical NSTX Ohmic plasma ( $\langle T_e \rangle \approx 0.25$  keV). (b) High-resolution spectrum around the 284 and 335 Å Mg- and Na-like Fe transitions.

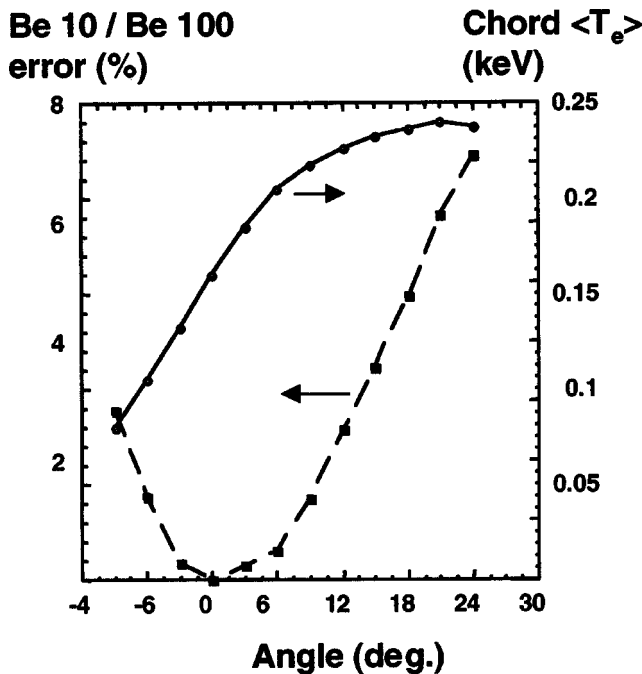


FIG. 9. Systematic error in the Be 10/Be 100 ratio due to the filter thickness increase with chord angle (Ohmic conditions). The chord averaged electron temperature is also shown.

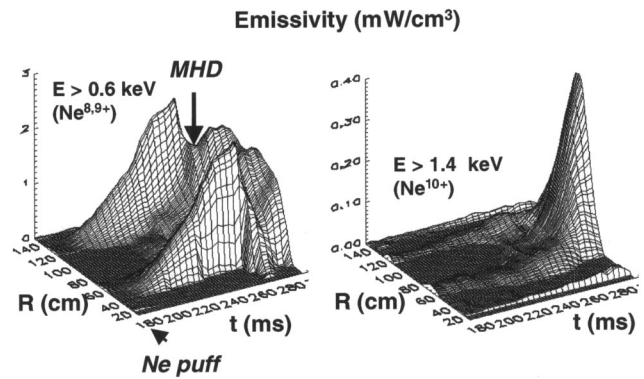


FIG. 10. Time evolution of neon emission recorded with Be 10 and Be 100 filters during neon injection in beam heated discharges. The neon contribution is obtained by subtracting the background C emission from consecutive reproducible discharge.

be partially accounted for through iterative calculations of the spectrum.

### C. Perturbative impurity transport measurements

As mentioned, estimating the absolute magnitude of the transport coefficients requires time-dependent (perturbative) measurements. We performed such measurements at NSTX by injecting brief neon puffs in beam heated discharges and following its penetration with the USXR array system in the multicolor configuration.<sup>9</sup> We chose neon because of its relatively low-Z and strong USXR emission. Since the dominant Ne charge states in the target plasma are fully stripped Ne<sup>10+</sup> in the core and He-, H-like Ne<sup>8,9+</sup> at  $r/a > 0.5$ , we discriminated between their spectral signatures ( $E > 1.4$  keV recombination continuum and  $E \approx 0.9-1.0$  keV line emission, respectively) by using the Be 10/Be 100 filter combination. Typical results are illustrated in Fig. 10, showing that a shell of Ne<sup>8,9+</sup> ions quickly forms at  $r/a \approx 0.6$ , but neither Ne<sup>8,9+</sup> nor Ne<sup>10+</sup> ions penetrate inside this radius over an extended period of time. Modeling this effect with the above package gives a diffusion coefficient in the neoclassical range, which suggests a low level of turbulent ion transport in NSTX.<sup>9</sup>

In conclusion, the tests of the impurity diagnostics package on NSTX show it can be a valuable tool for the study of sub-keV plasma. Further developments of the package include extension of the collisional-radiative HULLAC data for all impurities of interest and inclusion in the MIST code of the HULLAC computed ionization/recombination data.

### ACKNOWLEDGMENTS

The authors acknowledge the support of the NSTX Team in performing the above measurements. This work is supported by U.S. Doe Grant Nos. DE-FG02-99ER54523 and DE-FG02-86ER52314ATDoE at Johns Hopkins University.

<sup>1</sup>R. C. Isler, Fusion Eng. Des. **34-35**, 115 (1997).  
<sup>2</sup>E. S. Marmor *et al.*, Rev. Sci. Instrum. **72**, 940 (2001).  
<sup>3</sup>S. Kaye *et al.*, Phys. Plasmas **8**, 1977 (2001).  
<sup>4</sup>R. J. Taylor *et al.*, Bull. Am. Phys. Soc. **43**, 1825 (1998).  
<sup>5</sup>C. T. Hsu and D. J. Sigmar, Plasma Phys. Controlled Fusion **32**, 499 (1990).  
<sup>6</sup>L. C. Ingesson *et al.*, Nucl. Fusion **38**, 1675 (1998).

- <sup>7</sup>D. Stutman, M. Finkenthal, V. Soukhanovskii, M. J. May, H. W. Moos, and R. Kaita, *Rev. Sci. Instrum.* **70**, 572 (1999).
- <sup>8</sup>V. Soukhanovskii *et al.*, *Rev. Sci. Instrum.* **72**, 737 (2001).
- <sup>9</sup>D. Stutman *et al.*, Proceedings of the 29th European Physical Society Conference on Plasma Physics and Controlled Fusion, Montreux, Switzerland, Physical Society 17–21 June 2002, paper P4.06%.
- <sup>10</sup>B. Blagojevic, D. Stutman, M. Finkenthal, H. W. Moos, R. Kaita, and R. Majeski, *Rev. Sci. Instrum.* (these proceedings).
- <sup>11</sup>A. Bar-Shalom, M. Klapisch, and J. Oreg, *Phys. Rev. A* **38**, 1773 (1988).
- <sup>12</sup>M. J. May *et al.*, *Rev. Sci. Instrum.* **70**, 375 (1999).
- <sup>13</sup>E. H. Silver *et al.*, *Rev. Sci. Instrum.* **53**, 1198 (1982).
- <sup>14</sup>R. A. Hulse, *Nucl. Technol/Fusion* **3**, 259 (1983).
- <sup>15</sup>N. J. Lopez Cardozo, *Plasma Phys. Controlled Fusion* **37**, 799 (1995).
- <sup>16</sup>D. Stutman *et al.*, Proceedings of the 28th European Physical Society Conference on Plasma Physics and Controlled Fusion, 18–22 June 2001, Madeira, Portugal, paper P1.115.